

# Protein folding in a force-clamp

Marek Cieplak<sup>1</sup> and P. Szymczak<sup>2</sup>

<sup>1</sup>*Institute of Physics, Polish Academy of Sciences, Al. Lotników 32/46, 02-668 Warsaw, Poland*

<sup>2</sup>*Institute of Theoretical Physics, Warsaw University, ul. Hoża 69, 00-681 Warsaw, Poland*

Kinetics of folding of a protein held in a force-clamp are compared to an unconstrained folding. The comparison is made within a simple topology-based dynamical model of ubiquitin. We demonstrate that the experimentally observed variations in the end-to-end distance reflect microscopic events during folding. However, the folding scenarios in and out of the force-clamp are distinct.

Recent advances in nano-technology have enabled manipulation of single biomolecules, especially by means of the atomic force microscopy (AFM). The manipulation usually involves mechanical stretching and monitoring of the force of resistance as a function of displacement of the AFM tip. In 2001, Oberhauser et al.<sup>1</sup> have developed a force-clamp – a variant of AFM with an electronic adjustment of the tip displacement so that a constant pulling force is maintained. This technique allows one to measure the force dependence of the unfolding probability and has been used to probe the mechanical stability of two different domains of titin. The force-clamp microscopy has been subsequently developed by Fernandez and Li<sup>2</sup> to monitor the folding trajectory of a single protein that is first stretched by a constant unfolding force and then suddenly submitted to a substantially reduced force. The first tests on polyubiquitin have demonstrated a structured time dependence of the end-to-end distance,  $L$ . What this behavior corresponds to microscopically remains to be elucidated.

In this paper we ask what one can learn from monitoring  $L$  during folding of a protein under a small stress and, in particular, is this process related to folding that is taking place without any mechanical constraints? We address these questions theoretically by performing molecular dynamics simulations in a coarse-grained topology-based model<sup>4</sup>. Such a model is ideally suited to study conceptual questions about large conformational changes because it makes relevant time scales accessible to computations.

We focus on ubiquitin and two-ubiquitin since this case relates to the experimental studies<sup>2,3</sup>. A single ubiquitin consists of 76 amino acids and its structure is deposited in the Protein Data Bank<sup>5</sup> with a code 1ubq. The two-ubiquitin is modeled by linking two ubiquitins in a series through an extra peptide bond. We follow the implementation of the model along the lines outlined in refs.<sup>6</sup>.

In short, a protein is represented by a chain of  $C^\alpha$  atoms that are tethered by harmonic potentials with minima at 3.8 Å. The effective self-interactions between the atoms are either purely repulsive or are minimum-endowed-contacts of the Lennard-Jones type,  $V_{ij} = 4\epsilon \left[ \left( \frac{\sigma_{ij}}{r_{ij}} \right)^{12} - \left( \frac{\sigma_{ij}}{r_{ij}} \right)^6 \right]$ . The length parameters  $\sigma_{ij}$  are chosen so that the potential minima correspond, pair-by-pair, to the experimentally established native distances between the  $C^\alpha$  atoms in amino acids in the pair. The distinction between the two kinds of the interactions is established based on the absence or presence of overlaps between all other atoms in the  $i$  and  $j$  amino acids in the native conformation. The effective geometry of atoms in the tests for overlaps is assigned following a procedure advanced by Tsai et al.<sup>7</sup>. The repulsive interactions are described by the  $r_{ij}^{-12}$  part of the Lennard-Jones potential combined with a constant shift term that makes the potential vanish smoothly at  $\sigma = 5$  Å. It should be noted that the specificity of a protein is contained in the length parameters  $\sigma_{ij}$  and not in the energy parameter,  $\epsilon$ . The energy parameter is taken to be uniform and its effective value for titin and ubiquitin appears to be of order 900 K so the reduced temperature,  $\tilde{T} = k_B T / \epsilon$  of 0.3 ( $k_B$  is the Boltzmann constant and  $T$  is temperature) should be close to the room temperature value<sup>8</sup>. All of the simulations reported here were performed at this temperature. In our stretching simulations, the N-terminus of the protein is attached to harmonic springs of elastic constant  $k=0.06$   $\epsilon/\text{Å}^2$ . The C-terminus is pulled by a constant force,  $F$ . The dimensionless force,  $F\sigma/\epsilon$ , will be denoted by  $\tilde{F}$ .

Thermostating and mimicking some other effects of the solvent is provided by the Langevin noise. An equation of motion for each  $C^\alpha$  reads then  $m\dot{\mathbf{r}} = -\gamma\dot{\mathbf{r}} + F_c + \Gamma$ , where  $F_c$  is the net force on an atom due to the molecular potentials and  $\Gamma$  is a Gaussian noise term with dispersion  $\sqrt{2\gamma k_B T}$ . The damping constant  $\gamma$  is taken to be equal to  $2m/\tau$  and the dispersion of the random forces is equal to  $\sqrt{2\gamma k_B T}$ . This choice of  $\gamma$  corresponds to a situation in which the inertial effects are small<sup>6</sup> but the damping action is not yet as strong as in water. The more realistic damping is stronger by a factor of order 25 which extends the effective time scales by the same factor since the dependence of the folding times on  $\gamma$  is linear<sup>6</sup>. The equations of motion are solved by a fifth order predictor-corrector

scheme. The molecular dynamics time evolution is governed by the time unit  $\tau = \sqrt{m\sigma^2/\epsilon} \approx 3\text{ps}$  where  $m$  is the average mass of the amino acids. For our model of ubiquitin, the reduced temperature of melting is 0.23 and that of optimal folding 0.28 which indicates good unfrustrated kinetics and two-state folding behavior<sup>6</sup>. In an unfolded state there are no contacts and folding means increasing the number of contacts that get established. A contact between amino acids  $i$  and  $j$  is said to be established if the corresponding distance  $r_{ij}$  becomes less than  $1.5\sigma_{ij}$  (close to the inflection point of the Lennard-Jones potential). The folding time  $t_{fold}$  is defined as the first time at which all contacts are established simultaneously. (The condition of simultaneity necessarily involves longer time scales than those connected to single contact events).

Figure 1 illustrates examples of the experimental-like protocol that is adopted when studying force-clamped folding: a strong force of  $\tilde{F}=2$  is applied to induce unfolding and once this is accomplished, the force is reduced to a smaller value of  $\tilde{F}'=0.3$  to generate refolding; after refolding, the second such cycle of stretching and refolding is initiated, etc. Force induced unfolding – the first leg of the protocol – has been analyzed for ubiquitin theoretically before<sup>10,11</sup> and now we focus on what follows after the force quench. For single ubiquitin (the top two panels), there is a single jump in  $L$  during stretching, whereas for two-ubiquitin (the bottom panel)  $L$  increases in two steps, indicating a serial nature of unwinding – domain after domain. Figure 2 shows that the bigger the  $\tilde{F}'$ , the longer the mean refolding time,  $\langle t_{fold} \rangle$ . This also means the longer lasting intervals between noticeable shortenings of  $L$ . As it is seen in Fig. 1,  $L$  shrinks in an almost continuous fashion for  $\tilde{F}'=0.3$  whereas the steps are more pronounced and long lasting for  $\tilde{F}'=0.36$  because the larger stretching force generates a stronger impediment to folding.

It should be noted that even when  $\tilde{F}'=0$ , the folding process is not identical to a clamp-free folding because the N-terminus is connected to a spring that is anchored. The inset of Figure 2 shows that fixing one end of a protein delays folding nearly by a factor of 2. This seems to imply that diffusion-limited processes play an important role in the ubiquitin folding. Namely, according to the classical Smoluchowski result<sup>12</sup> the binding rate for a diffusion limited process is  $k_s = 4\pi Da$ , where  $D$  is the relative diffusion coefficient of a pair of reactants (amino acids) which are to make a contact once within a final distance of  $a$ . If one of them is immobile,  $D$  is halved and the time needed to form a contact increases accordingly. This argument is also consistent with the diffusion-collision model of Karplus and Weaver<sup>13</sup>. It is worth noting that for a shorter system, such as a single helix<sup>14</sup>, the situation is reversed: helix with a fixed end folds slightly faster than a free one. However, the diffusion is not a limiting process in the helix, since the sequential distance of aminoacids in the native contact in the helix does not exceed 4 and the process is energy driven. The factor of two difference in the folding time between free and clamped ubiquitin is also in a good agreement with the data obtained by Fernandez and Li<sup>2</sup> when an extrapolation to  $F' = 0$  is done and compared to the free ubiquitin folding times (see eg.<sup>15</sup> and references therein). Sosnick<sup>16</sup> interprets this difference in folding times as having origin in random nature of aggregation that partially unfolded molecules of ubiquitin may participate in when in a dense solution. The intimacy of protein chains would then give rise to the additional resistance to folding and hence to the longer times. Our results suggest that the aggregation mechanism is not necessary: single molecules themselves give rise to the phenomenon.

The distributions of the folding times both for free and clamped end are well fitted by the log-normal distribution except for large times where a transition to power-law-like tail is seen. Similar distributions were reported by Zhou et al.<sup>17</sup> for the free folding of  $\beta$ -hairpin fragment of protein G whereas the power law tails were predicted theoretically based on the energy landscape theory<sup>18</sup> and the hierarchically constrained dynamics model<sup>19</sup>.

It should be noted that the shape of the distribution reflects variations in the time scale of folding which are due to variations in the unfolded initial states, random character of the Langevin noise, and some variety in the shapes of final conformations that result when folding is declared accomplished. Such distributions exist for many simple proteins no matter which model of a protein is adopted.

There is a related implementation of the Go-like model<sup>20,21</sup> in which instead of the Lennard-Jones contact potentials combined with the chirality terms one considers the 10-12 contact potentials combined with potentials that involve the bond and dihedral angles. It has been shown<sup>21</sup> that the other implementation is endowed with an explicit two-state behavior since its free energy, at least for some proteins, has a two-minima form when plotted against the fraction,  $Q$ , of the established native contacts. In particular Zhang et al.<sup>22</sup> have demonstrated the thermodynamic two-state behavior for ubiquitin and Li et al.<sup>23</sup> have used it to study refolding upon force quench of titin and to show dependence on initial conditions. The technical differences between the two implementations do not translate into any qualitative differences in kinetics and thermodynamics<sup>24</sup> and our choice is motivated by a better computational efficiency.

Force-clamping results not only in longer folding but also in channeling the process through a modified pathway

even if  $\tilde{F}'=0$ . The kinetics of folding can be quantified with the use of the so called scenario diagrams<sup>6,25</sup> in which one plots an average time to establish a contact,  $t_c$ , against the contact order, i.e. against the sequential distance,  $j - i$ , between the amino acids that form a native contact. The left panels of Figure 3 compare the folding scenarios for the unconstrained and anchored (at the N terminus) single ubiquitin. The free case reveals folding that is fairly monotonic as a function of the contact order: the short-range contacts are established the first and the long-range contacts the last. When one end is held fixed, the sequence of events splits into more identifiable branches so that contacts of a given contact order are established at up to three distinct time scales. In addition, the order of events gets overturned. For instance, the hairpin at the N-terminus (solid squares) gets established now near the completion of folding, instead of at the beginning, despite the small sequential distances in the hairpin. Another difference is that there is no longer any time separation between linking the segment (17-27) with (51-59) (solid triangles) and connecting (36-44) to the strand (65-72) (open circles). The panels on the right hand side of Figure 3 make a similar comparison for a two-ubiquitin tandem arrangement and demonstrate that in the clamp-free folding process the folding events involve the two ubiquitins simultaneously. On the other hand, if one end is clamped, then the free-end domain folds first, as it can diffuse faster, and the domain that is close to the clamp folds next. Thus fixing one end induces seriality in folding. (We find that the same holds when a non-zero  $\tilde{F}'$  is applied).

The left panel of Figure 4 shows that application of the force at the C-terminus affects folding of a single ubiquitin even further. It restores the time separation between the events corresponding to the solid triangles and open circles; it makes the contacts with the helix (open triangles) take place at the very beginning of folding, instead of in the middle; it keeps establishing the hairpin throughout the process until the very end. We conclude that folding in a force-clamp is distinct both from folding that is not restricted mechanically and from folding that is partially restricted.

Another important aspect of the force-clamped folding is that its time scales are extended – the bigger the  $\tilde{F}'$ , the longer the folding time and, in particular, larger time intervals between individual events. This makes it easier for the atomic force microscopy to sense major events in folding, especially those that result in large time gaps between a next stage of contact formation. The right-hand panel of Figure 4 shows the distance  $L$  as a function of time for  $\tilde{F}'$ . The way the panel is plotted is rotated by  $90^\circ$  so that the time axis is parallel to that on the left-hand panel and it spans the same duration. It is seen that  $L$  varies in a discontinuous fashion forming a pattern of "punctuated equilibria". Furthermore, the jumps are very well correlated with the scenario diagram: the time gaps between establishment of subsequent contacts are reflected in a nearly constant value of  $L$  and a rapid chain of events make the  $L$  suddenly shorter. When the number of ubiquitins is larger than one (see Figure 1), the rapid changes in  $L$  are less pronounced since the unfolded modules act as soft entropic springs<sup>26</sup> whose length fluctuations tend to mask the decrease in the total  $L$ . As noted by Best and Hummer<sup>26</sup>, resolving kinetic events could be enhanced by operating at higher forces that reduce fluctuations. We concur and also point to the beneficial effects of the increased time scales in resolving the folding events.

In conclusion, results on our dynamical model suggest that monitoring the end-to-end distance in a force-clamp microscope does probe folding in a meaningful way. However, the folding process itself is different from that taking place without any mechanical constraints.

M.C. appreciates discussions with Julio Fernandez and Andrzej Sienkiewicz. This work was funded by the Ministry of Science in Poland (grant 2P03B 03225).

- 
- <sup>1</sup> A. F. Oberhauser, P. K. Hansma, M. Carrion-Vazquez, and J. M. Fernandez, *Proc. Natl. Acad. Sci. USA* **98**, 468 (2001).  
<sup>2</sup> J. M. Fernandez and H. Li, *Science* **303** 1674 (2004).  
<sup>3</sup> M. Schlierf, H. Li, J. M. Fernandez *Proc. Natl. Acad. Sci. USA*, **101**, 7299 (2004)  
<sup>4</sup> H. Abe and N. Go, *Biopolymers* **20** 1013 (1981); S. Takada, *Proc. Natl. Acad. Sci. (USA)* **96** 11698 (1999).  
<sup>5</sup> H.M. Berman, J. Westbrook, Z. Feng, G. Gilliland, T.N. Bhat, H. Weissig, I.N. Shindyalov, P.E. Bourne: *Nucleic Acids Research*, **28** 235 (2000).  
<sup>6</sup> T. X. Hoang and M. Cieplak, *J. Chem. Phys.* **113**, 8319-8328 (2000); M. Cieplak and T. X. Hoang, *Biophysical J.* **84** 475 (2003); M. Cieplak, T. X. Hoang and M. O. Robbins, *Proteins: Struct. Funct. Bio.* **56** 285 (2004).  
<sup>7</sup> J. Tsai, R. Taylor, C. Chothia, and M. Gerstein, *J. Mol. Biol.* **290** 253 (1999).  
<sup>8</sup> M. Cieplak, A. Pastore and T. X. Hoang, *J. Chem. Phys.* **122** 054906 (2004); M. Cieplak and P. E. Marszalek, *J. Chem. Phys.* **123**, 194903 (2005).  
<sup>9</sup> E. Evans *Faraday Discuss.* **111**, 16 (2003)  
<sup>10</sup> P. C. Li, and D. E. Makarov, *J. Chem. Phys.* **121**, 4826 (2004).

- <sup>11</sup> P. Szymczak and M. Cieplak, *J. Phys.: Cond. Mat.* **18** L21 (2006)
- <sup>12</sup> M. Smoluchowski, *Z. Phys. Chem.* **92**, 129 (1917); H.-X. Zhou *J. Mol. Recognit.* **17**, 368 (2004).
- <sup>13</sup> M. Karplus and D. L. Weaver, *Nature* **260**, 404 (1976).
- <sup>14</sup> T. X. Hoang and M. Cieplak, *J. Chem. Phys.* **112**, 6851 (2000).
- <sup>15</sup> B. A. Krantz, T. R. Sosnick *Biochemistry* **39**, 11696 (2000).
- <sup>16</sup> T. R. Sosnick, *Science* **306**, 411 (2004)
- <sup>17</sup> Y. Zhou, C. Zhang, G. Stell, J. Wang, *J. Am. Chem. Soc.* **125**, 6300 (2003).
- <sup>18</sup> C.-L. Lee, C.-T. Lin, G. Stell, J. Wang, energy *Phys. Rev. E* **67**, 041905 (2003).
- <sup>19</sup> M. Skorobogatiy, H. Guo, M. Zuckermann *J. Chem. Phys.* **109**, 2528 (1998).
- <sup>20</sup> T. Veitshans, D. Klimov, and D. Thirumalai, *Folding Des.* **2**, 1-22 (1997).
- <sup>21</sup> C. Clementi, H. Nymeyer, and J. N. Onuchic. *J. Mol. Biol.* **298**, 937 (2000).
- <sup>22</sup> J. Zhang, M. Qin and W. Wang, *Proteins: Struct. Funct. Bio.* **59**, 565 (2005).
- <sup>23</sup> M. S. Li, C-K. Hu, D. Klimov, and D. Thirumalai, *Proc. Natl. Acad. Sci. (USA)* **93** (2006).
- <sup>24</sup> M. Cieplak and Trinh Xuan Hoang, *Physica A* **330**, 195 (2003).
- <sup>25</sup> M. Cieplak, *Phys. Rev. E* **69**, 031907 (2004).
- <sup>26</sup> R. B. Best and G. Hummer, *Science* **308**, 498B (2005).

## FIGURE CAPTIONS

- Fig. 1.** Examples of  $L$  vs. time trajectories in two cycles of the force  $\tilde{F}$  varying in the following fashion:  $2-\tilde{F}'-2-\tilde{F}'$ , where the values of  $\tilde{F}'$  are indicated. The top two panels are for ubiquitin and the bottom panel for two-ubiquitin. The dashed line in the upper panel shows the time dependence of the stretching force in this case. The scale for  $\tilde{F}$  coincides with that of  $L/100$ .
- Fig. 2.** The mean folding time,  $\langle t_{fold} \rangle$ , as a function of  $\tilde{F}'$ . The inset shows distributions of folding times for 1ubq with one terminus fixed (the shaded histogram) and with free ends. The fits are to a log-normal distribution  $\frac{1}{\sqrt{2\pi\sigma(t-t_0)}} \exp\left(-\frac{\ln^2\left(\frac{t-t_0}{m}\right)}{2\sigma^2}\right)$ . The values of  $t_0/\tau$ ,  $\sigma$ , and  $m/\tau$  are 1050, 0.37, 820 and 480, 0.9, 215 respectively. The refolding time is measured from the drop in the force.
- Fig. 3.** Folding scenarios for a single ubiquitin (the left hand panel) and for two ubiquitins connected in tandem (the right hand panels) as averaged over 100 trajectories. The top panels correspond to unconstrained processes whereas the bottom panels to processes in which the N-terminus is fixed. The symbols assigned to specific contacts are the same in the panels on the left. Open circles, open triangles, open squares, open pentagons, solid triangles, and solid squares correspond to contacts (36-44)-(65-72), (12-17)-(23-34), [(1-7),(12-17)]-(65,72), (41-49)-(41-49), (17-27)-(51-59), (1-7)-(12-17) respectively. The crosses denote all other contacts. The segment (23-34) corresponds to a helix. The two  $\beta$ -strand (1-7) and ((12-17) form a hairpin. The remaining  $\beta$ -strands are (17-27), (41-49), and (51-59). In the panels on the right, we assign open circles to all contacts that exist in ubiquitin on the N-terminal side of the tandem arrangement whereas the solid triangles to contacts in the other ubiquitin.
- Fig. 4.** The left panel shows the scenario of folding for  $\tilde{F}'=0.36$ . The symbols used are like in the left panels of Figure 3. In a tandem arrangement of two ubiquitin at this force, there is a serial folding but the choice of the first ubiquitin to fold is random (not shown). The right panel shows the corresponding values of  $L$ , together with the snapshots of the conformations. The top snapshot is for the native conformation. The constant force is applied to the terminus shown on the right-hand side of the snapshot. The left-hand side terminus is attached to a fixed spring.

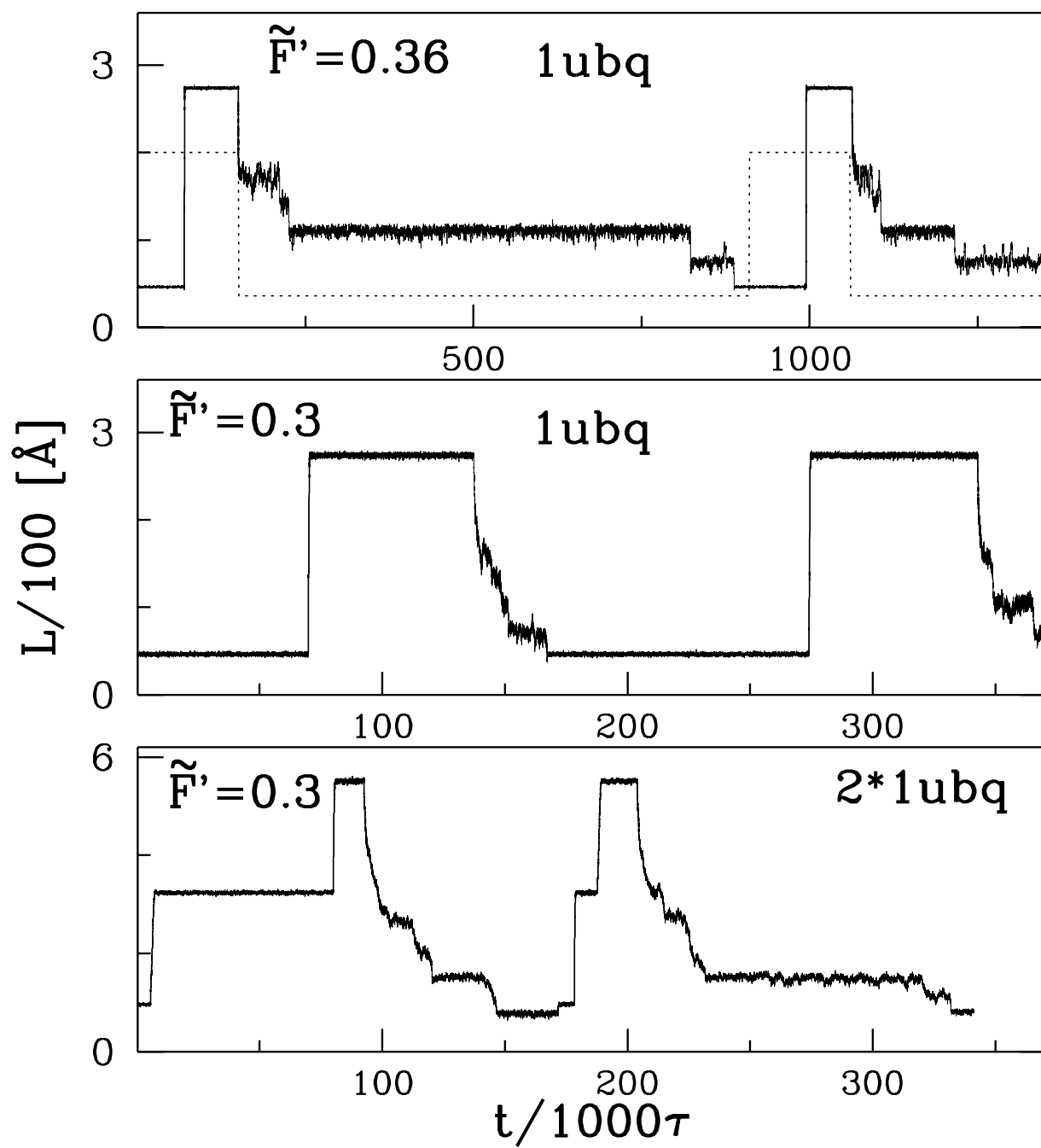


FIG. 1:

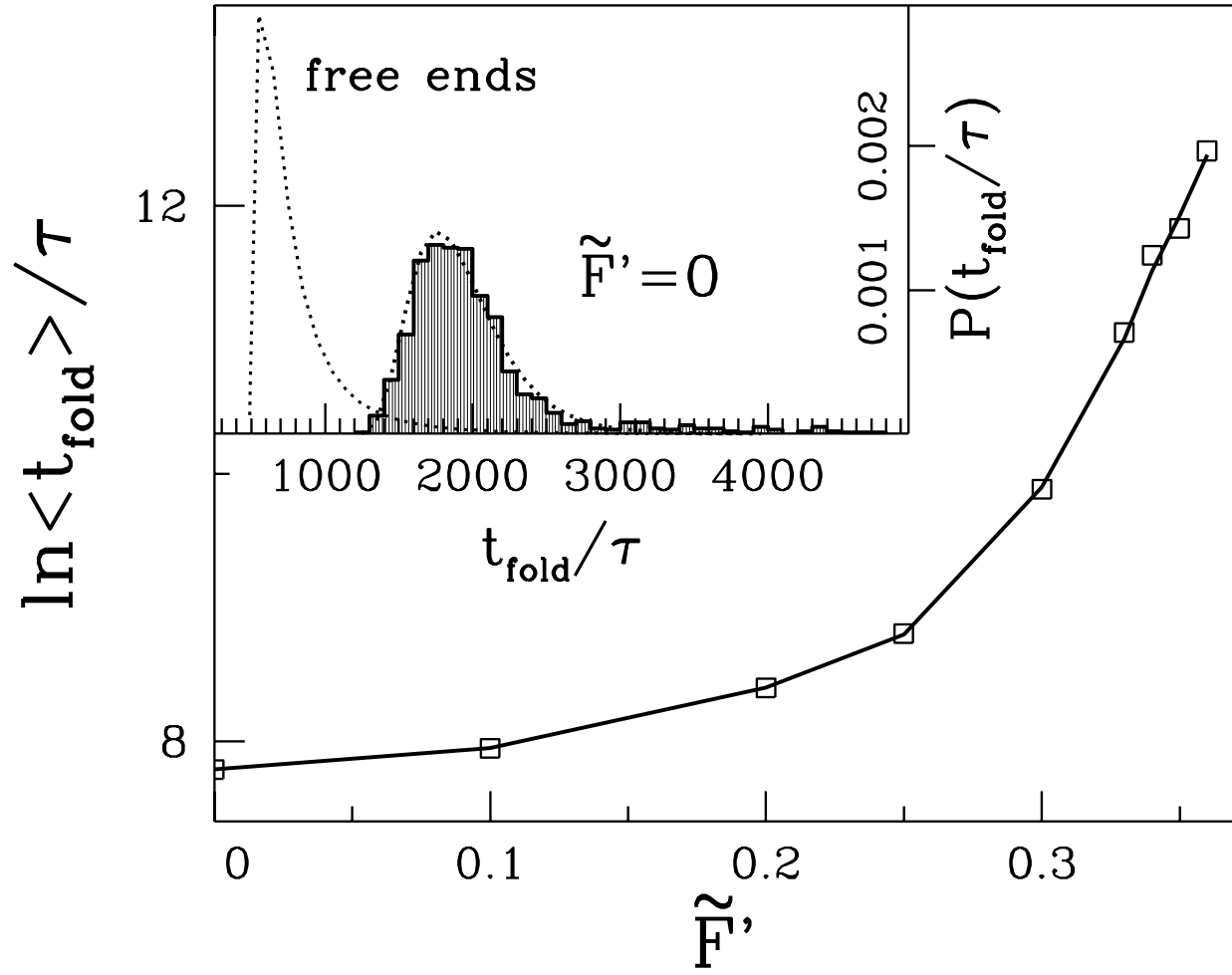


FIG. 2:

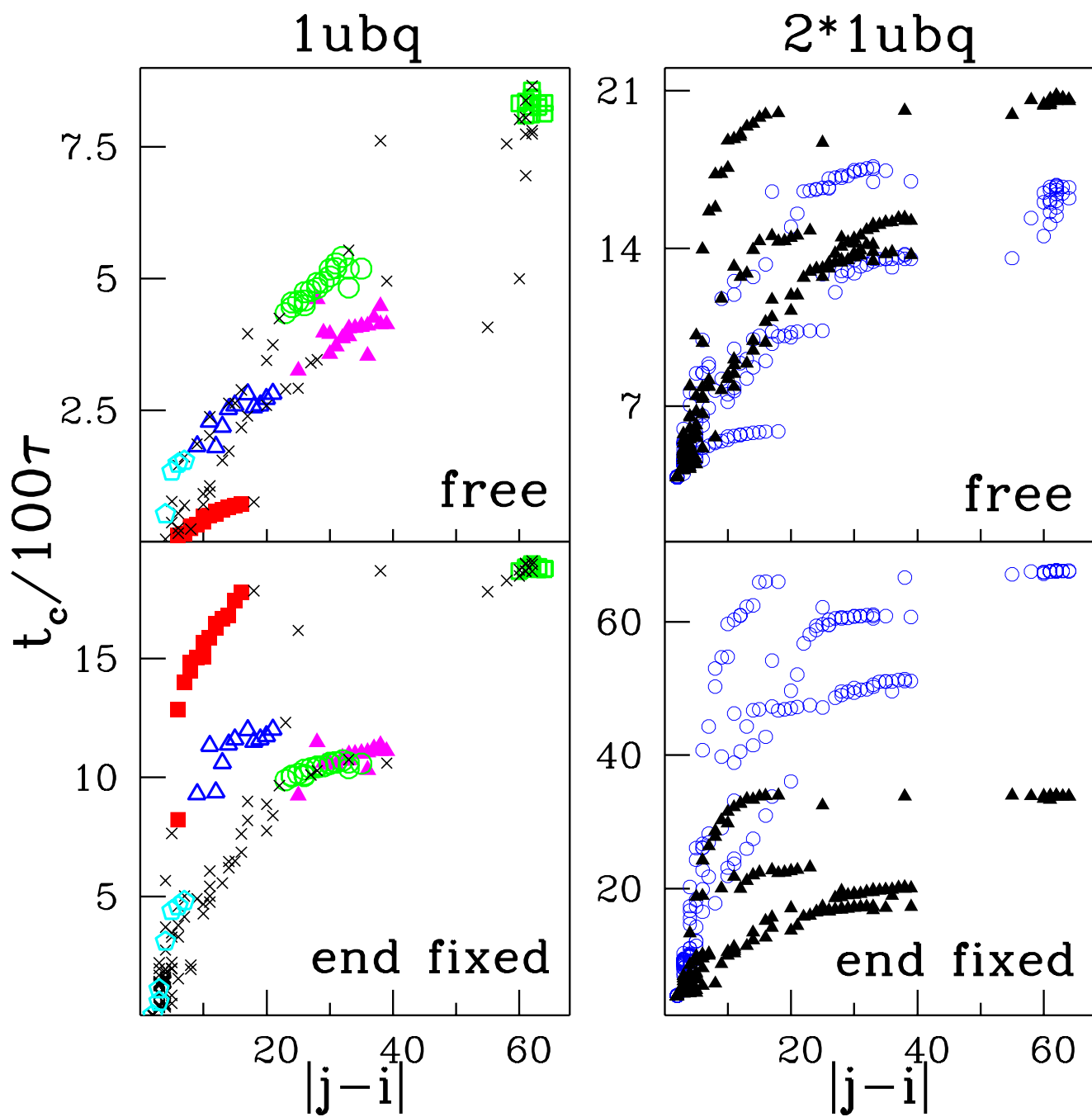


FIG. 3:

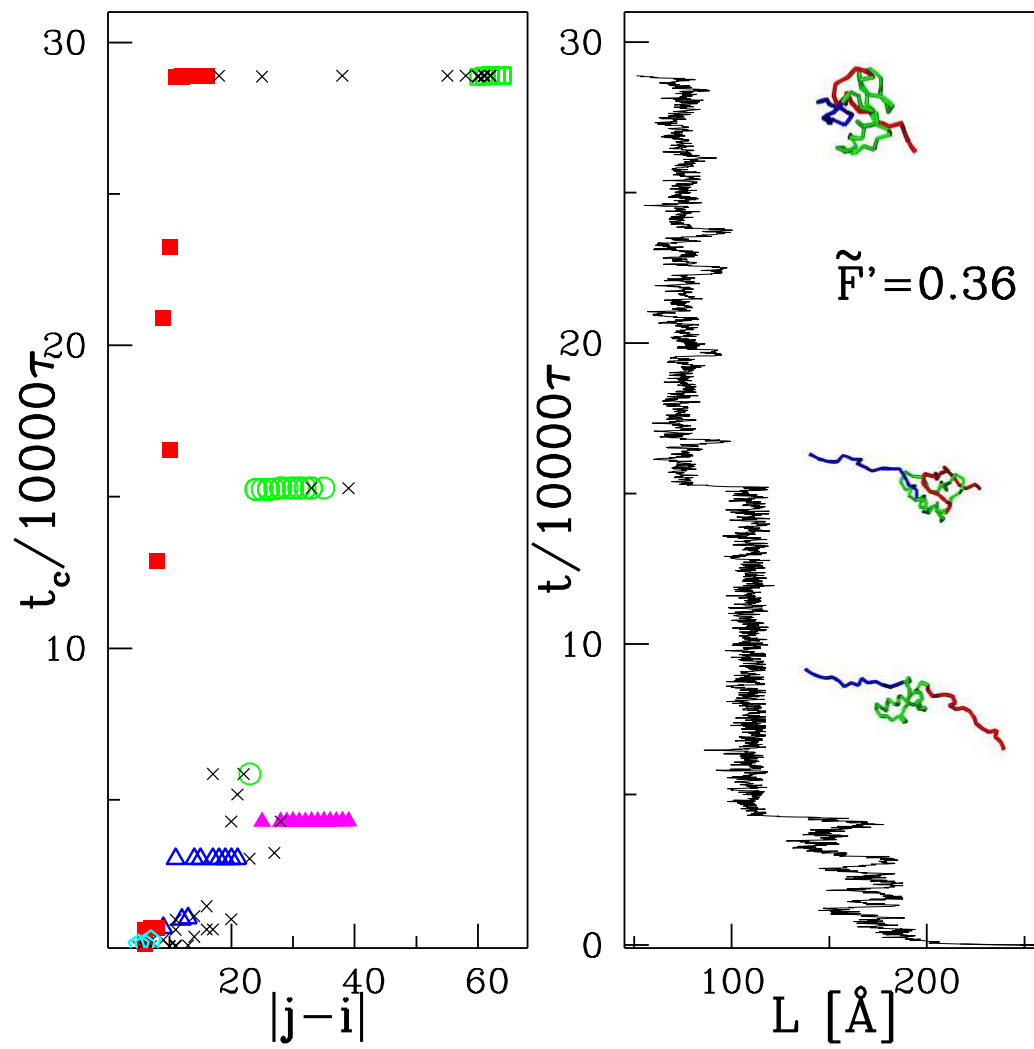


FIG. 4: